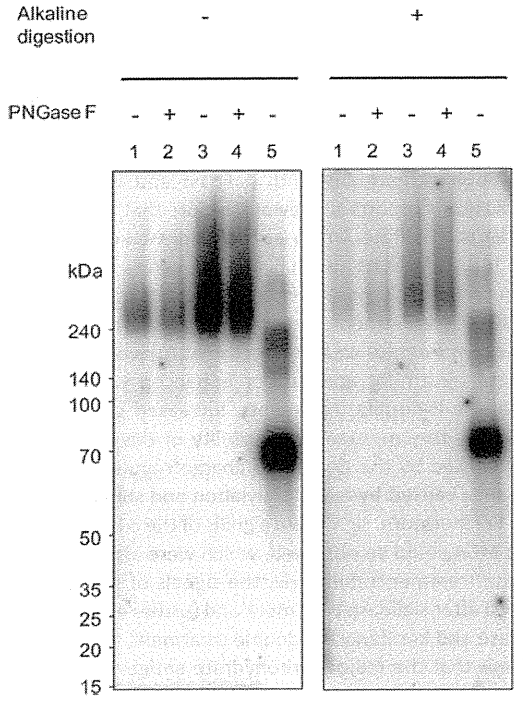

Figure 5. Glycan ligands on podocalyxin recognized by rBC2LCN are *O*-glycans. The podocalyxin immunoprecipitated from induced pluripotent stem cells (iPS201B7 [P45], 123; lanes 1 and 2) and embryonic stem cells (KhES-1 [P26], 156; lanes 3 and 4) with or without PNGase F treatment was run on 5%–20% acrylamide gel under reducing condition and transferred onto polyvinylidene difluoride membranes. The membranes were treated with phosphate-buffered saline (left panel) or 0.05 M NaOH (right panel) and blotted with horseradish peroxidase-conjugated rBC2LCN. Lane 5 shows Fucα1–2Galβ1–3GlcNAcβ1–3Galβ1–4Glc-BSA (rBC2LCN ligand, 0.5 μg). Abbreviation: PNGase F, Peptide:*N*-glycosidase F.

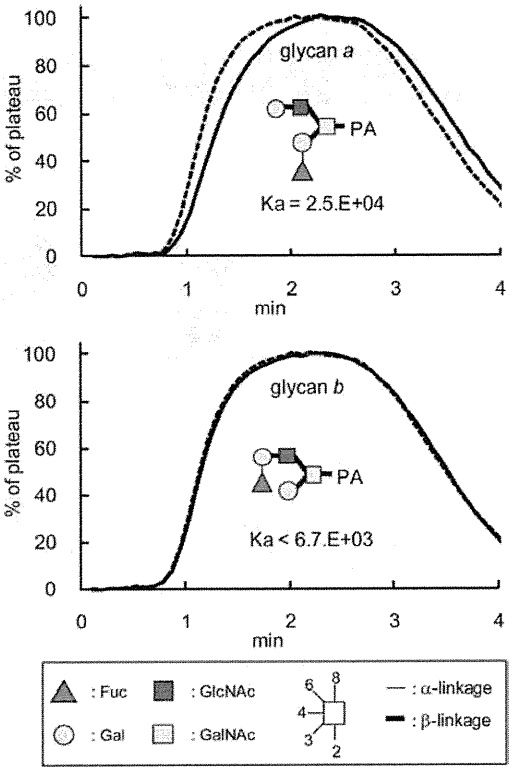

Figure 6. rBC2LCN binds to an *O*-glycan containing H type 3 isolated from induced pluripotent stem (iPS) cells. rBC2LCN was immobilized onto NHS-activated Sepharose 4FF (GE Healthcare) and packed into a miniature column and connected to a high-performance liquid chromatograph. PA glycans (glycans *a* and *b*, solid lines) prepared from human iPS cells (201B7) were injected into the column. The elution profile was then detected by fluorescence (excitation, 285 nm; emission, 350 nm). The elution front of PA glycan relative to that of negative control PA glycan (Manα1–6(Manα1–3)Manβ1–4GlcNAcβ1–4GlcNAc-PA, dotted line), referred to as V-V_0, was then determined. Woolf-Hofstee plots were prepared using the V-V_0 value. The intercept and slope of the fitted line represent B_t (nmol) and $-K_d$ (μM), respectively. Analysis of concentration dependence was performed using globo H (Fucα1–2Galβ1–3GalNAcβ1–3Galα1–4Galβ1–4Glc)-*p*-nitrophenol. Abbreviation: PA, pyridylaminated.

using a quantitative frontal affinity chromatography (FAC) technique [26] (Fig. 6). For comparison, its isomeric *O*-glycan containing an H type 2 structure (Fucα1–2Galβ1–4GlcNAcβ1–6(Galβ1–3)GalNAc-PA, designated glycan *b*), was analyzed, which was also prepared from 201B7 iPS cells. As a result, rBC2LCN was found to bind glycan *a* containing the H type 3 structure with a K_a of 2.5×10^4 M^{-1}, whereas no detectable binding was observed for the related glycan *b* containing the H type 2 structure ($K_a < 6.7 \times 10^3$ M^{-1}). Consistent with a recent study using glycan microarray [7], the present FAC analysis using 126 standard PA glycans confirmed that rBC2LCN bound to H type 1 (Fucα1–2Galβ1–3GlcNAcβ1–3Galβ1–4Glc-PA, $K_a = 2.8 \times 10^4$ M^{-1}) and Le^b (Fucα1–2Galβ1–3(Fucα1–4)GlcNAcβ1–3Galβ1–4Glc-PA, $K_a = 2.0 \times 10^5$ M^{-1}), but not to other glycans without the defined epitope structure Fucα1–2Galβ1–3GlcNAc(GalNAc). They include high-mannose-type, agalactosylated, galactosylated, sialylated *N*-glycans, and glycolipid-type glycans, demonstrating that rBC2LCN is highly specific to this glycan epitope (data not shown). Combined with the facts that podocalyxin is heavily *O*-glycosylated on its mucin domain and that podocalyxin binding to rBC2LCN was decreased by an alkaline treatment, it is most likely that the carbohydrate antigens on podocalyxin recognized by rBC2LCN are H type 3-containing *O*-glycans, such as glycan *a* isolated from iPS201B7 cells.

Discussion

Podocalyxin is a type I transmembrane sialoglycoprotein of the CD34 family, which was originally cloned from the human kidney as a component of the podocyte cell glycocalyx [28]. Later, podocalyxin was reported to act as a pluripotent stem cell marker, which is highly expressed on human ES cells [39–42]. Subsequently, podocalyxin was identified as a carrier molecule of the well-known pluripotency stem cell markers TRA-1-60 and TRA-1-81 [4]. In this study, we have clearly demonstrated that podocalyxin is a glycoprotein ligand of rBC2LCN, a novel probe for human pluripotent cells [7]. This indicates a possibility that podocalyxin functions as a ligand of both probes (TRA-1-60/81 and rBC2LCN) specific to human pluripotent stem cells.

In lectin-blotting analysis, rBC2LCN bound exclusively to undifferentiated human iPS cells and ES cells, but not at all to differentiated somatic cells, supporting the previous finding that rBC2LCN is highly specific to pluripotent stem cells [7]. Surprisingly, podocalyxin was found to be the major glycoprotein ligand of rBC2LCN in human iPS cells and ES cells. However, this could be explained by the unique molecular nature of podocalyxin,

that is, highly expressed in pluripotent stem cells and heavily glycosylated, whereas altered glycosylation machinery upon induction of pluripotency should affect various glycoproteins rather than a specific one. In fact, rBC2LCN-positive bands were detected from 70 to 140 kDa (Fig. 2), but their contribution is rather small compared with podocalyxin. Notably, the podocalyxin protein was detectable at a similar degree in iPS cells and ES cells, whereas the rBC2LCN reactivity was varied among the cell types of iPS cells and ES cells. In this context, it is interesting to speculate that the rBC2LCN reactivity might correlate with the degree of differentiation of pluripotent stem cells.

Alkaline digestion, but not PNGase F treatment, reduced the binding of rBC2LCN to podocalyxin, indicating that the carbohydrate antigens on podocalyxin are presented partly on *O*-glycans. Previously, we have performed quantitative glycome analysis targeting both *N*- and *O*-glycans of undifferentiated iPS cells (201B7) and differentiated human dermal fibroblasts by a glycosidase-assisted HPLC method combined with mass spectrometry [38]. Among 47 types of *N*- and *O*-glycans identified from iPS cells, a potential carbohydrate antigen of rBC2LCN was identified, with an *O*-glycan-carrying H type 3 epitope structure (Fucα1–2Galβ1–3(Galβ1–3GlcNAcβ1–6)GalNAc-PA), whereas H type 1 could not be detected on either *N*- and *O*-glycans. Indeed, rBC2LCN bound to this *O*-glycan with a K_a of 2.5×10^4 M^{-1}. Even though the binding affinity of rBC2LCN to glycan *a* is relatively weak (K_a of 2.5×10^4 M^{-1}), the affinity to podocalyxin is expected to be increased, because of the high density of the glycan ligands expressed on podocalyxin by a so-called "glycan cluster effect" [43]. Altogether, these results indicate that H type 3 is a most probable human pluripotency marker, which is expressed exclusively in undifferentiated iPS cells [38] and is recognized by rBC2LCN.

Podocalyxin has important roles in cell morphology, adhesion, and migration in a variety of tissues including kidney podocytes, hematopoietic progenitors, vascular endothelia, and a subset of neurons [44]. In the developing kidney, podocalyxin plays an essential role in the formation and maintenance of podocyte foot processes [44]. Podocalyxin-null mice fail to form foot processes and slit diaphragms and thus exhibit profound defects in kidney development and die within 24 hours of birth with anuric renal failure [45]. The ectopic expression of podocalyxin induces morphologic changes including actin recruitment and the formation of microvillus and foot process in a manner dependent of its extracellular domain [44]. Podocalyxin coats the secondary foot processes of the podocytes and functions to open the urinary filtration barrier by keeping adjacent foot processes separated by its negative charge. Podocalyxin is also expressed in the hematopoietic system and is involved in cell migration [44]. In addition, podocalyxin is abnormally expressed in subsets of breast, prostate, liver, pancreatic, and kidney cancer, as well as leukemia, and is likely involved in metastasis [44]. Although the biological functions of podocalyxin in stem cells and its relationship with pluripotency are largely unknown, it is likely that podocalyxin regulates the maintenance and morphology of stem cells as well [4]. It would be of interest to investigate how changes of glycan structures on podocalyxin affect its protein and/or cellular functions. Indeed, partial loss-of-function mutation in the gene encoding glycoprotein-*N*-acetylgalactosamine-3-β-galactosyltransferase (C1GalT1), an enzyme essential for the synthesis of core1 (Galβ1–3GalNAc), which is the precursor of H type 3 (Fucα1–2Galβ1–3GalNAc), was reported to cause kidney diseases including distortion of the glomerular-tubular architecture [46]. In these mice, podocalyxin is the major underglycosylated protein, and its appropriate glycosylation was implicated to be essential for kidney functions. Therefore, it is likely that altered glycosylation affects both the chemical and physical properties of podocalyxin as well as its recognition molecules, leading to the modification and regulation of cell-cell communications, which is important for the maintenance of pluripotency.

Conclusion

We conclude that podocalyxin is the glycoprotein ligand of rBC2LCN in human iPS and ES cells. The carbohydrate antigens of rBC2LCN are expressed on *O*-glycans of podocalyxin, since alkaline hydrolysis greatly reduced the binding of rBC2LCN to human iPS cells and ES cells. rBC2LCN bound to an *O*-glycan carrying H type 3 epitope structure isolated from iPS cells, suggesting that H type 3 is a novel pluripotency glycan marker. Further studies will be crucial to understand the roles of glycans of podocalyxin for pluripotency and self-renewal of human iPS cells and ES cells.

Acknowledgments

We thank Dr. Atsushi Kuno and Dr. Yoko Itakura for advice and discussion and Yoshiko Kubo, Jinko Murakami, Yasuhiko Aiki, and Dr. Kumiko Higuchi for technical assistance. Dr. Hiromi Ito provided the globo H (Fucα1–2Galβ1–3GalNAcβ1–3Galα1–4Galβ1–4Glc)-*p*-nitrophenyl. This work was supported in part by the New Energy and Industrial Technology Development Organization in Japan. Human iPS cells (201B7) were obtained from RIKEN Bioresource Center. K.N. is currently affiliated with the Faculty of Medicine, University of Tsukuba, Tsukuba, Ibaraki, Japan.

Author Contributions

H.T.: conception and design, manuscript writing, data analysis and interpretation; A.M., K. Hiemori, and K. Hasehira: data analysis and interpretation; Y.O., Y. Ito, K.N., M.O., S.T., Mahito Nakanishi, Y. Ikehara, Mio Nakanishi, K.O., T.C., M.T., H.A., and A.U.: provision of study material or patients; M.A.: provision of study material or patients, financial support; J.H.: manuscript writing.

Disclosure of Potential Conflicts of Interest

The authors indicate no potential conflicts of interest.

References

1 Muramatsu T, Muramatsu H. Carbohydrate antigens expressed on stem cells and early embryonic cells. Glycoconj J 2004;21:41–45.

2 Andrews PW. Toward safer regenerative medicine. Nat Biotechnol 2011;29:803–805.

3 Lanctot PM, Gage FH, Varki AP. The glycans of stem cells. Curr Opin Chem Biol 2007; 11:373–380.

4 Schopperle WM, DeWolf WC. The TRA-1-60 and TRA-1-81 human pluripotent stem cell markers are expressed on podocalyxin in embryonal carcinoma. Stem Cells 2007;25:723–730.

5 Natunen S, Satomaa T, Pitkanen V et al. The binding specificity of the marker antibodies Tra-1-60 and Tra-1-81 reveals a novel pluripotency associated type 1 lactosamine epitope. Glycobiology 2011;21:1125–1130.

6 Tang C, Lee AS, Volkmer JP et al. An antibody against SSEA-5 glycan on human

pluripotent stem cells enables removal of teratoma-forming cells. Nat Biotechnol 2011;29:829–834.

7 Tateno H, Toyota M, Saito S et al. Glycome diagnosis of human induced pluripotent stem cells using lectin microarray. J Biol Chem 2011; 286:20345–20353.

8 Sulák O, Cioci G, Delia M et al. A TNF-like trimeric lectin domain from Burkholderia cenocepacia with specificity for fucosylated human histo-blood group antigens. Structure 2010;18:59–72.

9 Onuma Y, Tateno H, Hirabayashi J et al. rBC2LCN, a new probe for live cell imaging of human pluripotent stem cells. Biochem Biophys Res Commun 2013;431:524–529.

10 Kuno A, Kato Y, Matsuda A et al. Focused differential glycan analysis with the platform antibody-assisted lectin profiling for glycan-related biomarker verification. Mol Cell Proteomics 2009;8:99–108.

11 Nishino K, Toyoda M, Yamazaki-Inoue M et al. Defining hypo-methylated regions of stem cell-specific promoters in human iPS cells derived from extra-embryonic amnions and lung fibroblasts. PLoS One 2010;5:e13017.

12 Nagata S, Toyoda M, Yamaguchi S et al. Efficient reprogramming of human and mouse primary extra-embryonic cells to pluripotent stem cells. Genes Cells 2009;14:1395–1404.

13 Takahashi K, Tanabe K, Ohnuki M et al. Induction of pluripotent stem cells from adult human fibroblasts by defined factors. Cell 2007;131:861–872.

14 Makino H, Toyoda M, Matsumoto K et al. Mesenchymal to embryonic incomplete transition of human cells by chimeric OCT4/3 (POU5F1) with physiological co-activator EWS. Exp Cell Res 2009;315:2727–2740.

15 Toyoda M, Yamazaki-Inoue M, Itakura Y et al. Lectin microarray analysis of pluripotent and multipotent stem cells. Genes Cells 2011; 16:1–11.

16 Saito S, Onuma Y, Ito Y et al. Possible linkages between the inner and outer cellular states of human induced pluripotent stem cells. BMC Syst Biol 2011;5(suppl 1):S17.

17 Nishimura K, Sano M, Ohtaka M et al. Development of defective and persistent Sendai virus vector: A unique gene delivery/expression system ideal for cell reprogramming. J Biol Chem 2011;286:4760–4771.

18 Suemori H, Yasuchika K, Hasegawa K et al. Efficient establishment of human embryonic stem cell lines and long-term maintenance with stable karyotype by enzymatic bulk passage. Biochem Biophys Res Commun 2006; 345:926–932.

19 Osafune K, Caron L, Borowiak M et al. Marked differences in differentiation propensity among human embryonic stem cell lines. Nat Biotechnol 2008;26:313–315.

20 Tateno H, Kuno A, Itakura Y et al. A versatile technology for cellular glycomics using lectin microarray. Methods Enzymol 2010;478: 181–195.

21 Duk M, Ugorski M, Lisowska E. Beta-Elimination of O-glycans from glycoproteins transferred to immobilon P membranes: Method and some applications. Anal Biochem 1997; 253:98–102.

22 Kato Y, Hayatsu N, Kaneko MK et al. Increased expression of highly sulfated keratan sulfate synthesized in malignant astrocytic tumors. Biochem Biophys Res Commun 2008; 369:1041–1046.

23 Kuno A, Uchiyama N, Koseki-Kuno S et al. Evanescent-field fluorescence-assisted lectin microarray: A new strategy for glycan profiling. Nat Methods 2005;2:851–856.

24 Uchiyama N, Kuno A, Tateno H et al. Optimization of evanescent-field fluorescence-assisted lectin microarray for high-sensitivity detection of monovalent oligosaccharides and glycoproteins. Proteomics 2008;8:3042–3050.

25 Itakura Y, Nakamura-Tsuruta S, Kominami J et al. Systematic comparison of oligosaccharide specificity of *Ricinus communis* agglutinin I and *Erythrina lectins*: A search by frontal affinity chromatography. J Biochem 2007;142:459–469.

26 Tateno H, Nakamura-Tsuruta S, Hirabayashi J. Frontal affinity chromatography: Sugar-protein interactions. Nat Protoc 2007;2: 2529–2537.

27 Nakamura S, Yagi F, Totani K et al. Comparative analysis of carbohydrate-binding properties of two tandem repeat-type Jacalin-related lectins, *Castanea crenata* agglutinin and *Cycas revoluta* leaf lectin. FEBS J 2005;272: 2784–2799.

28 Kershaw DB, Beck SG, Wharram BL et al. Molecular cloning and characterization of human podocalyxin-like protein: Orthologous relationship to rabbit PCLP1 and rat podocalyxin. J Biol Chem 1997;272:15708–15714.

29 Schopperle WM, Armant DR, DeWolf WC. Purification of a tumor-specific PNA-binding glycoprotein, gp200, from a human embryonal carcinoma cell line. Arch Biochem Biophys 1992;298:538–543.

30 Takeda T, Go WY, Orlando RA et al. Expression of podocalyxin inhibits cell-cell adhesion and modifies junctional properties in Madin-Darby canine kidney cells. Mol Biol Cell 2000;11:3219–3232.

31 Kerjaschki D, Vernillo AT, Farquhar MG. Reduced sialylation of podocalyxin—the major sialoprotein of the rat kidney glomerulus—in aminonucleoside nephrosis. Am J Pathol 1985; 118:343–349.

32 Dekan G, Gabel C, Farquhar MG. Sulfate contributes to the negative charge of podocalyxin, the major sialoglycoprotein of the glomerular filtration slits. Proc Natl Acad Sci USA 1991;88:5398–5402.

33 Kerjaschki D, Sharkey DJ, Farquhar MG. Identification and characterization of podocalyxin—the major sialoprotein of the renal glomerular epithelial cell. J Cell Biol 1984;98: 1591–1596.

34 Yamagishi K, Suzuki K, Imai K et al. Purification, characterization, and molecular cloning of a novel keratan sulfate hydrolase, endo-beta-N-acetylglucosaminidase, from *Bacillus circulans*. J Biol Chem 2003;278:25766–25772.

35 Yabe R, Itakura Y, Nakamura-Tsuruta S et al. Engineering a versatile tandem repeat-type alpha2–6sialic acid-binding lectin. Biochem Biophys Res Commun 2009;384:204–209.

36 Seko A, Ohkura T, Ideo H et al. Novel O-linked glycans containing 6′-sulfo-Gal/GalNAc of MUC1 secreted from human breast cancer YMB-S cells: Possible carbohydrate epitopes of KL-6(MUC1) monoclonal antibody. Glycobiology 2012;22:181–195.

37 Kochibe N, Matta KL. Purification and properties of an N-acetylglucosamine-specific lectin from *Psathyrella velutina* mushroom. J Biol Chem 1989;264:173–177.

38 Hasehira K, Tateno H, Onuma Y et al. Structural and quantitative evidence for dynamic glycome shift upon production of human induced pluripotent stem cells. Mol Cell Proteomics 2012;11:1913–1923.

39 Richards M, Tan SP, Tan JH et al. The transcriptome profile of human embryonic stem cells as defined by SAGE. STEM CELLS 2004; 22:51–64.

40 Bhattacharya B, Miura T, Brandenberger R et al. Gene expression in human embryonic stem cell lines: Unique molecular signature. Blood 2004;103:2956–2964.

41 Zeng X, Miura T, Luo Y et al. Properties of pluripotent human embryonic stem cells BG01 and BG02. STEM CELLS 2004;22:292–312.

42 Hayman MW, Przyborski SA. Proteomic identification of biomarkers expressed by human pluripotent stem cells. Biochem Biophys Res Commun 2004;316:918–923.

43 Dam TK, Gerken TA, Brewer CF. Thermodynamics of multivalent carbohydrate-lectin cross-linking interactions: Importance of entropy in the bind and jump mechanism. Biochemistry 2009;48:3822–3827.

44 Nielsen JS, McNagny KM. The role of podocalyxin in health and disease. J Am Soc Nephrol 2009;20:1669–1676.

45 Doyonnas R, Kershaw DB, Duhme C et al. Anuria, omphalocele, and perinatal lethality in mice lacking the CD34-related protein podocalyxin. J Exp Med 2001;194:13–27.

46 Alexander WS, Viney EM, Zhang JG et al. Thrombocytopenia and kidney disease in mice with a mutation in the C1galt1 gene. Proc Natl Acad Sci USA 2006;103:16442–16447.

See www.StemCellsTM.com for supporting information available online.

International Journal of Nanomedicine

Dovepress
open access to scientific and medical research

Open Access Full Text Article

ORIGINAL RESEARCH

Enhanced in vivo osteogenesis by nanocarrier-fused bone morphogenetic protein-4

Yasuyuki Shiozaki[1,2]
Takashi Kitajima[4]
Tetsuro Mazaki[1,2]
Aki Yoshida[1]
Masato Tanaka[1]
Akihiro Umezawa[5]
Mariko Nakamura[6]
Yasuhiro Yoshida[3]
Yoshihiro Ito[4]
Toshifumi Ozaki[1]
Akihiro Matsukawa[2]

[1]Department of Orthopedic Surgery, Okayama University, Okayama, Okayama, Japan; [2]Department of Pathology and Experimental Medicine, Okayama University, Okayama, Okayama, Japan; [3]Department of Biomaterials, Graduate School of Medical, Dentistry, and Pharmaceutical Sciences, Okayama University, Okayama, Okayama, Japan; [4]Nano Medical Engineering Laboratory, RIKEN, Wako, Saitama, Japan; [5]National Research Institute for Child Health and Development, Okura, Tokyo, Japan; [6]Department of Health and Welfare Program, Kibi International University Junior College, Takahashi, Okayama, Japan

Correspondence: Akihiro Matsukawa
Department of Pathology and Experimental Medicine, Graduate School of Medical, Dentistry and Pharmaceutical Sciences, Okayama University 2-5-1, Shikata, Kita-ku, Okayama 700-8558, Japan
Tel +81 86 235 7141
Fax +81 86 235 7148
Email amatsu@md.okayama-u.ac.jp

Purpose: Bone defects and nonunions are major clinical skeletal problems. Growth factors are commonly used to promote bone regeneration; however, the clinical impact is limited because the factors do not last long at a given site. The introduction of tissue engineering aimed to deter the diffusion of these factors is a promising therapeutic strategy. The purpose of the present study was to evaluate the in vivo osteogenic capability of an engineered bone morphogenetic protein-4 (BMP4) fusion protein.

Methods: BMP4 was fused with a nanosized carrier, collagen-binding domain (CBD), derived from fibronectin. The stability of the CBD-BMP4 fusion protein was examined in vitro and in vivo. Osteogenic effects of CBD-BMP4 were evaluated by computer tomography after intramedullary injection without a collagen–sponge scaffold. Recombinant BMP-4, CBD, or vehicle were used as controls. Expressions of bone-related genes and growth factors were compared among the groups. Osteogenesis induced by CBD-BMP4, BMP4, and CBD was also assessed in a bone-defect model.

Results: In vitro, CBD-BMP4 was retained in a collagen gel for at least 7 days while BMP4 alone was released within 3 hours. In vivo, CBD-BMP4 remained at the given site for at least 2 weeks, both with or without a collagen–sponge scaffold, while BMP4 disappeared from the site within 3 days after injection. CBD-BMP4 induced better bone formation than BMP4 did alone, CBD alone, and vehicle after the intramedullary injection into the mouse femur. Bone-related genes and growth factors were expressed at higher levels in CBD-BMP4-treated mice than in all other groups, including BMP4-treated mice. Finally, CBD-BMP4 potentiated more bone formation than did controls, including BMP4 alone, when applied to cranial bone defects without a collagen scaffold.

Conclusion: Altogether, nanocarrier-CBD enhanced the retention of BMP4 in the bone, thereby promoting augmented osteogenic responses in the absence of a scaffold. These results suggest that CBD-BMP4 may be clinically useful in facilitating bone formation.

Keywords: BMP4, bone repair, bone tissue engineering, osteogenesis

Introduction

Bone defects and nonunions remain considerable problems caused by tumor and trauma, and their treatment constitutes a major challenge in orthopedic reconstitution surgery.[1] Autologous bone graft is a standard technique for inducing bone repair; however, clinical benefits are not ensured, and collateral symptoms, including persistent site pain, nerve injury, hematoma, infection, and fracture, frequently occur.[2] Recent advances in the treatment methods include the use of sophisticated biocompatible scaffolds, multipotential cell populations and appropriate cellular stimulation at the

submit your manuscript | www.dovepress.com
Dovepress
http://dx.doi.org/10.2147/IJN.S44174

affected sites. Currently, growth factor-based bone tissue engineering has attracted increasing attention.

Many growth factors induce osteogenesis.[3] Bone morphogenetic proteins (BMPs) are members of the transforming growth factor-β (TGFβ) protein superfamily, and are known to play pivotal roles in the regulation of bone induction, maintenance, and repair.[4,5] The US Food and Drug Administration has approved two BMPs – BMP2, and BMP7/OP1 – which have accompanied orthopedic surgery and are applied with an absorbable collagen sponge. The clinical benefits of BMP2 and BMP7 have been reported;[6,7] however, several reports described the heterotopic ossification associated with the use of BMP2 and BMP7.[8–10] To prevent heterotopic bone formation and induce successful site specific bone growth requires an approach that limits the diffusion of factors to target tissues.

BMP4 induces osteogenic differentiation of osteoblasts and osteoprogenitors and promotes bone formation,[11] thus playing a crucial role in the onset of bone and cartilage development and fracture repair.[12] In vivo BMP4 gene therapy accelerated the repair of bone fractures,[13] and performed as well or better when compared with BMP2.[14] Thus, BMP4 appears to be a viable other approach for treatment of bone defects and nonunions. BMP4 alone can be delivered by direct injection into the site of concern, but immobilized BMP4 can be localized and retained in the targeted site for longer periods and thus extend the functional half-life of this factor. Very recently, we have created a novel collagen-poly lactic-co-glycolic acid hybrid scaffold with a BMP4 fused to an additional collagen-binding domain (CBD) derived from fibronectin (CBD-BMP4).[15] CBD-BMP4 exhibited stronger and more stable collagen-binding activity than did wild type BMP4. This fusion protein, bound to a collagen-coated scaffold, induced osteogenic differentiation of human mesenchymal stem cells when these cells were implanted into nude mice.[15]

In the present study, we extend our previous work and demonstrate that CBD-BMP4 is retained longer at the targeted sites compared to BMP4 alone and induced augmented bone formation even when injected without scaffold. Considering that the 100 kDa of fibronectin fragment that includes CBD (45 kDa) was reported to be about 24 nm,[16] CBD size can be regarded as a nanocarrier. When applied to cranial bone defects, CBD-BMP4 successfully induced new and accelerated bone formation as compared to BMP4 alone. Thus, CBD-BMP4 may be promising for the treatment of bone defects and nonunions.

Materials and methods

CBD-BMP4

CBD-BMP4 fusion protein was prepared as described.[15] In brief, the recombinant protein was produced by transgenic silkworms, which carried a chimeric gene encoding CBD of human fibronectin and human BMP4 (mature form). The enterokinase recognition sequence was inserted between the CBD and BMP4 sequences. The fusion protein produced by and secreted into cocoons was extracted with $CaCl_2$ and affinity-purified by Gelatin Sepharose 4B (GE Healthcare, Waukesha, WI, USA). CBD protein (without BMP4 fusion) was prepared as described.[17] Control BMP4 was purchased from R&D Systems, Inc (Minneapolis, MN, USA). For some experiments, CBD-BMP4, BMP4, and CBD were labeled with HiLyte Fluor 555 (Dojindo Molecular Technologies, Inc, Kumamoto, Japan), according to the manufacturers' instructions. In brief, NH_2-reactive HiLyte Fluor 555 dissolved in 10 μL dimethyl sulfoxide was mixed with CBD-BMP4, BMP4, or CBD solution (10 μg protein in 100 μL of phosphate buffered saline [PBS]). The protein-dye solution was incubated for 10 minutes at 37°C and unreacted free dye was removed by centrifugation (8000 × g, 10 minutes) using a provided filtration tube. The labeled protein was then recovered from the filter membrane.

Characterization of CBD-BMP4

Purified protein was digested with enterokinase (EK Max, Life Technologies, Carlsbad, CA, USA), fractionated on sodium dodecyl sulfate-polyacrylamide gel, and transferred to a polyvinylidene difluoride membrane. The gel was stained with Coomassie Brilliant Blue. The membrane was incubated with anti-BMP4 goat serum (R&D Systems, Inc), followed by incubation with horseradish peroxidase-linked antigoat immunoglobulin G antibody (Vector Laboratories, Inc, Burlingame, CA, USA), and visualized using the ECL system (GE Healthcare). To assess binding stability, CBD-BMP4 or BMP4 was mixed with 0.2% collagen solution in Eagle's minimal essential medium, pH 7.4 (Koken Co, Tokyo, Japan), and the mixture (30 μL) was gelled at 37°C for 1 hour. PBS (150 μL) was then added and the overlaid PBS was collected after 1 hour, 3 hours, 1 day, 3 days, and 7 days. Protein released into PBS solution was dot-blotted to a nitrocellulose membrane, followed by immunostaining with goat anti-BMP4 and the secondary antibody, as above. The reaction was visualized using 4-chloronaphthol as a horseradish peroxidase substrate.

Animals

New Zealand White rabbits (female, 2.0 kg–2.5 kg) were purchased from Shimizu Laboratory Supplies (Kyoto, Japan). BALB/c mice (female, 6–8 weeks) were obtained from Charles River Laboratories (Yokohama, Japan). Animals were housed in a temperature-controlled environment with a 12-hour light/12-hour dark cycle under specific pathogen-free conditions and allowed free access to water and food. The animal care and use committee at Okayama University approved all animal experiments conducted in this study.

Collagen–sponge scaffold model

Rabbits were anesthetized with an intramuscular injection of ketamine (80 mg/kg). Both knees were shaved and draped in a sterile fashion, and a medial incision was made. A bone hole was made in the distal diaphysis of the femur with a φ5.0 mm drill, and a collagen sponge (3 mm cylinder, atelocollagen sponge, MIGHTY; Koken Co, Tokyo, Japan) was intramedullary implanted though the hole. The collagen sponge was presoaked with CBD-BMP4, BMP4, or CBD solution, and contained 1 μg of each protein. A sponge soaked with vehicle PBS alone was used as a control. These four groups of collagen sponges were randomly implanted into rabbit femurs (ten rabbits, 20 femurs, five femurs per each group). Rabbits were then housed in each cage without knee immobilization until the time of evaluation. Rabbits were sacrificed 4 weeks later, and the collagen sponge was retrieved from the femur, fixed in 10% formalin, decalcified in 10% ethylenediaminetetraacetic acid (EDTA), embedded in paraffin, and the sections were stained with hematoxylin–eosin. Histological sections were digitalized under a microscope, and the ossification area in the sponge was measured by image-analyzing software, WinROOF (Mitani Corp, Fukui, Japan). The peripheral area of each sponge was deselected to exclude bone ingrowth by spontaneous healing. To assess the retainment of CBD-BMP4, BMP4, or CBD in vivo, a collagen sponge containing 1 μg of each protein fluorescently labeled was implanted as described above. Sponges soaked with vehicle PBS alone were used as controls (six rabbits, 12 femurs, three femurs per each group). On days 1, 3, and 14 after the implantation, rabbits were killed, and the sponge was removed, frozen in Super CryoEmbedding Medium compound (Section-Lab Co, Hiroshima, Japan) and cut with a tungsten blade at –20°C, as described.[18] The sections were stained with calcein acetomethoxy (40 μg/mL; Dojindo Molecular Technologies) for bony calcium detection and evaluated under a fluorescence microscope.

Intramedullary injection model

Mice were anesthetized with ketamine (100 mg/kg). Both knees were shaved, and the skin was cleaned with 70% ethanol. A bone hole was made in the distal diaphysis of the femur with a 24 G needle, and CBD-BMP4, BMP4, or CBD (100 ng in 10 μL PBS) was injected into the medullary cavity of the right femur with a 27 G needle-tipped syringe. The left femur injected with 10 μL PBS was used as a control (five mice per each group). At 4 weeks after the injection, the mice were sacrificed, and the femurs were resected. The femurs were scanned by microcomputed tomography (micro-CT) (LaTheta LCT-200; Hitachi Aloka Medical, Ltd, Tokyo, Japan) using 48 μm slices (0.3 mm interval), and the bone mineral density (BMD) of individual trabecular bone area was calculated by accompanying image-analyzing software, LaTheta v1.20. In some mice, the bone marrow was washed with saline and the cells were stored at –80°C for messenger ribonucleic acid (mRNA) expression study. To assess the retainment of CBD-BMP4, BMP4, or CBD in vivo, each protein fluorescently labeled (1 μg in 10 μL PBS) or vehicle (10 μL PBS) was directly injected into the femur as described above (three mice per group). Mice were sacrificed on day 1, 3, and 14 after the injection and nondecalcification femurs were cut with a tungsten blade at –20°C, and the sections were stained with calcein acetomethoxy and evaluated under a fluorescence microscope.

Bone defect model

Bone defects were made in the cranial bone, as previously described.[19] Briefly, mice were anesthetized with ketamine (100 mg/kg), and the cranial bone was exposed. Bone defects were made in the parietal bone with a φ3.0 mm drill. After washing with saline, CBD-BMP4, BMP4, CBD (100 ng in 5 μL PBS), or vehicle (5 μL PBS), was applied to the defects, and the scalp was closed (five mice per each group). At 2 weeks after the surgery, the mice were killed, and the cranial bone was scanned by micro-CT in 48 μm slices. To analyze the ossification area, regions of interest were set on the bone defect area, and the accumulation of dots (counts per pixel) in the selected region of interest was measured using image-analyzing software (WinROOF; Mitani Corp). Three-dimensional images were reconstructed by the image-processing software, OsiriX (Pixmeo SARL, Bernex, Switzerland). Subsequently, the defect area was resected, fixed in 10% formalin, decalcified in 10% EDTA, embedded in paraffin, and the sections were stained with hematoxylin–eosin.

Quantitative real-time PCR

Samples were homogenized in lysis buffer (QuickGene; Fujifilm, Tokyo, Japan), and total ribonucleic acid (RNA) was isolated, according to the manufacturer's instructions. First-strand complementary deoxyribonucleic acid (cDNA) was constructed from 2 μg of total RNA with oligo (dT) as primers,[12–18] and the cDNAs were used as a template for polymerase chain reaction (PCR). Quantitative real-time PCR was performed with SYBR PCR master mix (Agilent Technologies, Santa Clara, CA, USA) and specific primers. To validate the SYBR Green PCR products, a dissociation step was done to verify the T_m (annealing temperature) of the SYBR Green PCR product after the PCR were run. The expression levels of each mRNA were normalized by the expression of a housekeeping gene hypoxanthine phosphoribosyltransferase. The primers used in this study are listed in Table 1.

Statistical analysis

Statistical analyses were performed using Student's *t*-test for paired samples and analysis of variance for multiple samples. All data were expressed as the mean ± standard error of the mean. $P < 0.05$ was considered statistically significant.

Table 1 Primers for quantitative real-time PCR

Gene	Orientation	Primer sequence (5′ to 3′)
ALP	Forward	TGAGCGACACGGACAAGA
	Reverse	GGCCTGGTAGTTGTTGTGAG
BSP	Forward	TTCCCAGGTGTGTCATTGAAGA
	Reverse	GGTATGTTTGCGCAGTTAGCAA
Osterix	Forward	GGAGGTTTCACTCCATTCCA
	Reverse	TAGAAGGAGCAAGGGGACAGA
Osteocalcin	Forward	GCCATCACCCTGTCTCCTAA
	Reverse	GCTGTGGAGAAGACACACGA
Runx2	Forward	GCCGGGAATGATGAGAACTA
	Reverse	GGACCGTCCACTGTCACTTT
BMP2	Forward	ACGTCCTCAGCGAATTTGAG
	Reverse	GCCTGCGGTACAGATCTAGC
BMP4	Forward	GCCGGAGGGCCAAGCGTAGCC CTAAG
	Reverse	CTGCCTGATCTCAGCGGCACCC ACATC
TGFβ	Forward	CAACAATTCCTGGCGTTACCTTGG
	Reverse	GAAAGCCCTGTATTCCGTCTCCTT
HPRT	Forward	TGACACTGGCAAAACAATGCA
	Reverse	GGTCCTTTTCACCAGCAAGCT

Abbreviations: PCR, polymerase chain reaction; ALP, alkaline phosphatase; BSP, bone sialoprotein; Runx, runt-related transcription factor; BMP, bone morphogenetic protein; TGF, transforming growth factor; HPRT, hypoxanthine phosphoribosyltransferase.

Results

Characterization of CBD-BMP4

Recombinant CBD-BMP4 was purified from cocoons of transgenic silkworms. Calculated molecular sizes of CBD-BMP4, CBD, and BMP4 moieties were 52.5 kDa, 39 kDa, and 13 kDa, respectively. As confirmed by enterokinase digestion, this fusion protein consisted of CBD and BMP4. BMP4 moiety released from CBD was immunoreactive with an anti-BMP4 antibody (Figure 1A). In in vitro experiments, CBD-BMP4 in a collagen gel was entrapped and localized for at least 7 days while unfused BMP4 diffused out of the gel as early as 1 hour and was undetectable after 1 day (Figure 1B), indicating that CBD-BMP4 showed much higher collagen-binding affinity than did BMP4.

Enhanced bone formation in collagen–sponge scaffold

We next asked whether CBD-BMP4 could display enhanced collagen-binding capacity in vivo and promote bone

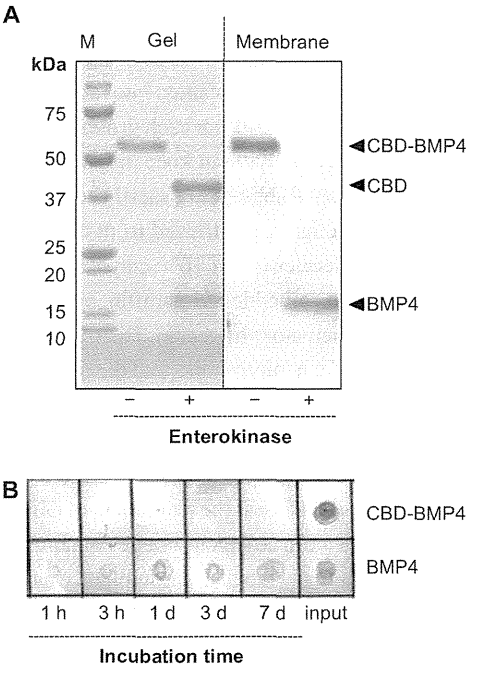

Figure 1 Characterization of CBD-BMP4. (**A**) Purified CBD-BMP4 was digested with enterokinase, fractionated on SDS-polyacrylamide gel, and transferred to a PVDF membrane. The gel was stained with Coomassie Brilliant Blue (left), and the membrane was immunoblotted with anti-BMP4 (right). (**B**) BMP4 or CBD-BMP4 was mixed with collagen solution, and the mixture was gelled at 37°C for 1 hour.
Note: Protein released into PBS solution was blotted to a nitrocellulose membrane and immunodetected with anti-BMP4.
Abbreviations: CBD, collagen-binding domain; BMP4, bone morphogenetic protein-4; SDS, sodium dodecyl sulfate; PVDF, polyvinylidene difluoride; PBS, phosphate buffered saline.

formation more effectively than BMP4 alone. To examine this, collagen sponges containing 1 μg of CBD-BMP4, BMP4, or CBD were placed in the rabbit femur, as described in the Methods section. The immunohistological data in Figure 2 demonstrated that BMP4 was found localized on day 1, but was no longer visible on day 3 after the implantation. A scant calcification was seen on day 14 (Figure 2).

In the case of CBD-BMP4, a stronger signal was seen on day 1 relative to BMP4, and the signal intensity did not diminish by day 3. Results with CBD alone were similar to those of the fusion protein at day 3. Of note was the finding that only CBD-BMP4 appeared to induce robust calcification in the site at day 14 (Figure 2). In another set of experiments, histological examination 4 weeks later revealed that CBD-BMP4 induced a thicker trabecular bone formation than BMP4 did (Figure 3A). Further, the ossification area formed by CBD-BMP4 injected animals was significantly larger than seen in BMP4 injected animals (Figure 3B). CBD induced slightly augmented bone formation as compared to the PBS control. These data clearly showed that CBD-BMP4 is retained longer at the given site in vivo, and induced bone formation more effectively than BMP4, CBD, or PBS when the fusion protein was implanted with scaffold.

Augmented bone formation without scaffold

Collagen is the major constituent of the bone matrix.[20] The above data prompted us to investigate whether CBD-BMP4 could remain at the given site without scaffold, leading to an augmented bone formation. To address this, we first confirmed the retainment of CBD-BMP4, BMP4, and CBD after a direct injection of fluorescence-labeled proteins (1 μg in 10 μL PBS) into the medullary cavity of mouse femur. The data in Figure 4 demonstrated that BMP4 was

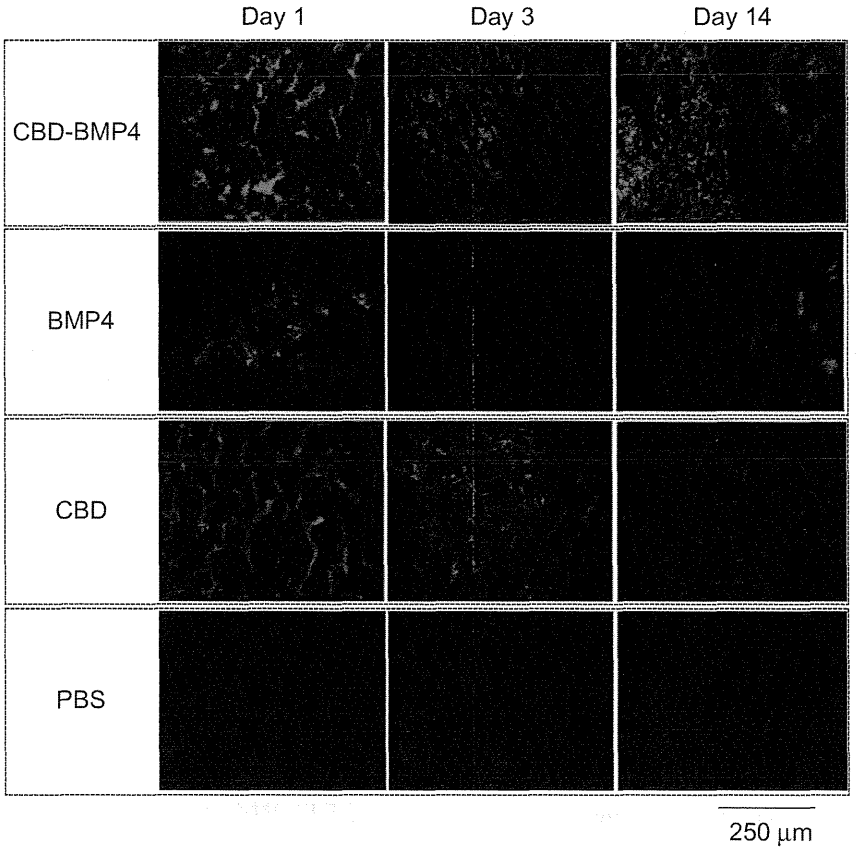

Figure 2 Fluorescence images of a collagen sponge.
Notes: Collagen sponges containing fluorescence-labeled CBD-BMP4, BMP4, or CBD were implanted into rabbit femur. Sponges soaked with vehicle PBS were used as a control (three femurs per each group). On days 1, 3, and 14 after the implantation, the sponges were retrieved, and the sections were examined under a fluorescence microscope. HiLyte Fluor 555-labeled CBD-BMP4/BMP4/CBD is shown in red. Bone stained by calcein acetomethoxy is shown in green. Representative photographs from each group are shown.
Abbreviations: CBD, collagen-binding domain; BMP4, bone morphogenetic protein-4; PBS, phosphate buffered saline.

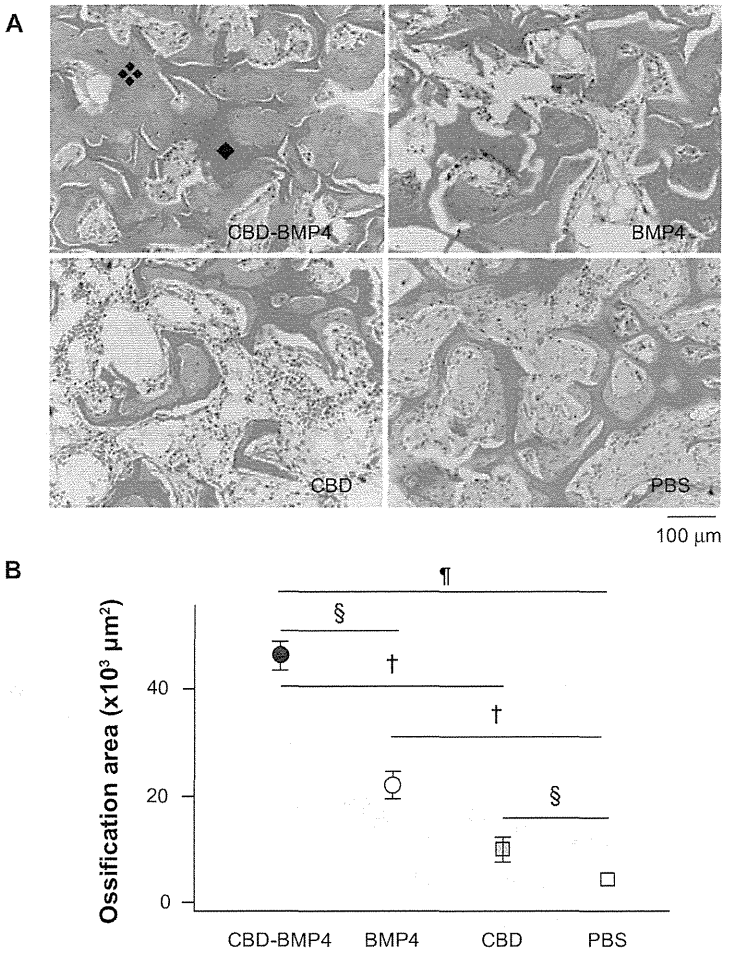

Figure 3 CBD-BMP4 augments new bone formation when delivered by collagen sponges. Collagen sponges containing 1 μg of CBD-BMP4, BMP4, and CBD were implanted into rabbit femurs. Sponges soaked with vehicle PBS were used as a control (five femurs per each group). Four weeks later, the sponge was retrieved, fixed, decalcified, and the sections were stained with HE. (**A**) Histological sections of the collagen sponge. Representative photographs of each group are shown. ❖: New bone (note osteocyte). ◆: Collagen sponge. (**B**) Ossification area in the sponge was calculated (five femurs per each group).
Notes: §$P < 0.05$; †$P < 0.01$; $P < 0.0001$. Magnification is shown by the bar (100 μm).
Abbreviations: CBD, collagen-binding domain; BMP4, bone morphogenetic protein-4; PBS, phosphate buffered saline; HE, hematoxylin and eosin stain.

not found on day 3 after the injection, whereas CBD-BMP4 was observed even after day 14. CBD remained in a similar fashion. Apparent calcification was seen only next to CBD-BMP4 on day 14 (Figure 4), suggesting enhanced new bone formation by CBD-BMP4.

We then assessed BMD by measuring micro-CT images (Figure 5A). BMD in mice treated with CBD-BMP4 at 4 weeks later was increased compared to BMP4, CBD and PBS groups. There was no difference between the BMP4 and PBS groups. BMD in CBD groups was higher than was seen in PBS groups (Figure 5B). The BMD in CBD-BMP4 and BMP4 groups were also measured at 8 weeks after the injection and showed that BMD in CBD-BMP4 groups was higher than that observed in BMP4 groups (Figure 5C). BMD in the CBD-BMP4 groups at 8 weeks increased as compared to that at 4 weeks (737.1 ± 8.1 mg/cm^3 versus 703.5 ± 5.9 mg/cm^3; respectively, $P < 0.05$, five mice each). No change was found in BMP4 groups (Figure 5C), suggesting prolonged osteogenic activity with CBD-BMP4. These data indicate that a single injection of CBD-BMP4 augments bone formation even without scaffold.

Osteogenic gene expressions by CBD-BMP4

To better understand the molecular mechanisms underlying the augmented osteogenesis by intramedullary CBD-BMP4 treatment, bone marrow cells were harvested from the femurs at 4 weeks after therapy injection and mRNA expression of osteogenic factors were examined. Osteoblast-associated factors including alkaline phosphatase (ALP), bone sialoprotein

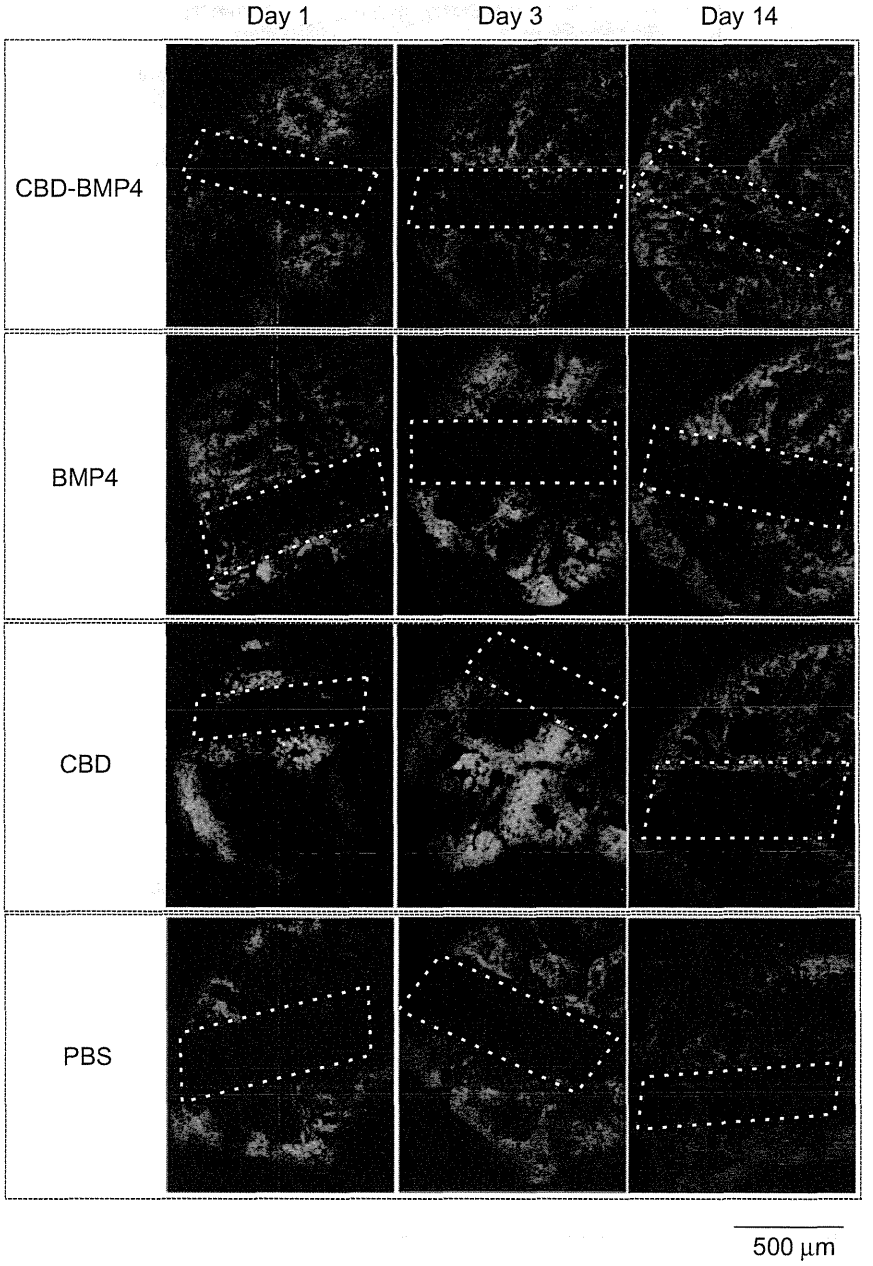

Figure 4 Fluorescence images of mouse femur.
Notes: Fluorescence-labeled CBD-BMP4, BMP4 or CBD (1 μg in 10 μL PBS) were injected into mouse femurs. PBS alone (10 μL) was used as a control (three mice per each group). On day 1, 3, and 14 after the injection, the femurs were resected, frozen, cut, and examined under a fluorescence microscope. HiLyte Fluor 555-labeled CBD-BMP4/BMP4/CBD is shown in red. Bone stained by calcein acetomethoxy is shown in green. Bone hole is shown in a dashed line. Shown were representative photographs from each group. Magnification is shown by the bar (500 μm).
Abbreviations: CBD, collagen-binding domain; BMP4, bone morphogenetic protein-4; PBS, phosphate buffered saline.

(BSP), osteocalcin, osterix, and Runt-related transcription factor 2 (Runx2) were expressed at higher levels in the CBD-BMP4 group than in the other groups, including the BMP4 group (Figure 6A).

In contrast, there was no difference between the BMP4 group and the PBS control. Interestingly, the CBD group showed increased ALP, BSP, and osteocalcin expression relative to the control PBS (Figure 6A). Endogenous expression of growth factors was examined next, which demonstrated that the CBD-BMP4 group, but not the BMP4 group, upregulated the expression of BMP2 and BMP4, as compared to PBS control. Augmented expression

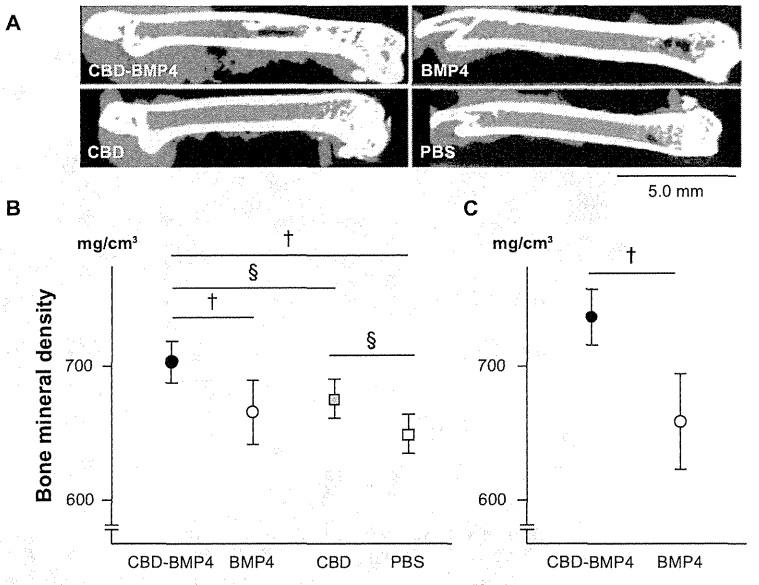

Figure 5 CBD-BMP4 accelerates bone mineral density. CBD-BMP4, BMP4, CBD (100 ng in 10 μL PBS), or vehicle PBS (10 μL) were directly injected into mouse femurs (five mice per each group). At 4 weeks after the injection, the femurs were scanned by micro-CT. (**A**) Representative images from each group. Bone mineral density was calculated by micro-CT at (**B**) 4 weeks and (**C**) 8 weeks after the injection.
Notes: §$P < 0.05$; †$P < 0.01$.
Abbreviations: CBD, collagen-binding domain; BMP4, bone morphogenetic protein-4; PBS, phosphate buffered saline; CT, computed tomography.

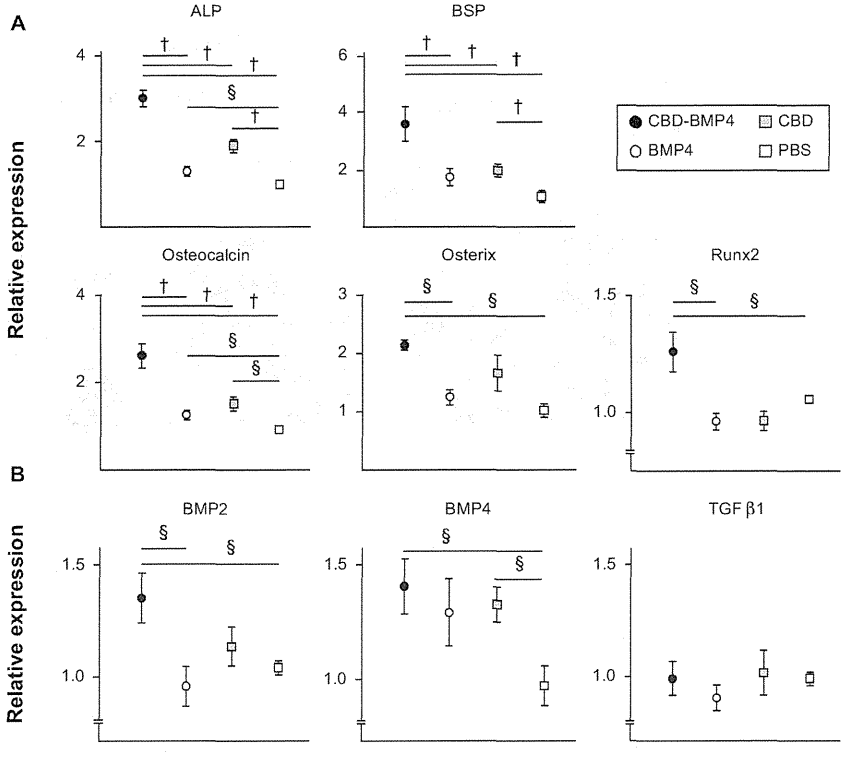

Figure 6 CBD-BMP4 increases osteogenic gene expression. Bone marrow cells were harvested at 4 weeks after the injection of CBD-BMP4, BMP4, CBD (100 ng in 10 μL PBS), or vehicle PBS (10 μL) (five mice per each group). mRNA expression for (**A**) osteoblast-associated factors and (**B**) bone growth factors were quantitated by RT-PCR. The expression levels of mRNA were normalized to HPRT.
Notes: §$P < 0.05$; †$P < 0.01$.
Abbreviations: CBD, collagen-binding domain; BMP4, bone morphogenetic protein-4; ALP, alkaline phosphatase; BSP, bone sialoprotein; PBS, phosphate buffered saline; RT-PCR, reverse transcription polymerase chain reaction; HPRT, hypoxanthine phosphoribosyltransferase.

of BMP4 was also found in the CBD group. No change was found in the expression level of TGFβ (Figure 6B). Thus, enhanced bone formation in the CBD-BMP4 group was associated with augmented expressions of osteogenic factors and growth factors. The BMP4 alone group failed to augment these factors during this time period (4 weeks after the injection), possibly due to the diffusion from the site (Figure 4). CBD, which was also present at the targeted site over a longer period, might stimulate bone formation by inducing endogenous BMP4.

Accelerated bone formation in a cranial bone defect model

To further strengthen the in vivo osteogenesis induced by CBD-BMP4, we applied CBD-BMP4, BMP4, CBD, or vehicle in a cranial bone defect model without scaffold. BMP4 treatment demonstrated new bone formation on day 14 after the treatment (Figure 7A). Obviously, CBD-BMP4 showed substantial ingrowth of new bone formation. As shown in Figure 7B, the ossification area induced by CBD-BMP4 and BMP4 was statistically increased as compared to that by PBS control. Importantly, there was more new bone formation in the CBD-BMP4-treated group than that in the BMP4 group. Ossification area by CBD was similar to that of the PBS control (Figure 7B). Histological examination consistently demonstrated new bone formation lined by a layer of osteoblasts in the CBD-BMP4- and the BMP4-treated group, which was more prominent in the CBD-BMP4 group (Figure 7C).

Discussion

Immobilized growth factors targeting the extracellular matrix (ECM) can be more effective than diffusible, free growth factors.[21] The goal of engineering a fusion protein was to deliver a functional substance that had limited diffusion over a prolonged period of time. Our novel BMP4 fusion protein with a nanosized carrier – namely, the CBD – seems to fulfill this requirement.[15] The stable binding of CBD to collagen led us to investigate whether this novel CBD-BMP4 by itself could enhance bone formation using bone matrix collagen as an innate scaffold.

As expected, CBD-BMP4 induced stronger bone formation than did BMP4. CBD-BMP4 remained at the injected site for at least 2 weeks, possibly through the CBD binding to bone matrix collagen, and the results demonstrated that new bone formation continues to be observed even after 8 weeks. There exist several kinds of gene-engineered binding growth factors, including BMPs.[21] Our CBD-BMP4 has advantages over other engineered fusion proteins. First, CBD-BMP4 induced entopic bone formation without using scaffold. As far as we know, this is the first report demonstrating accelerated bone formation by a fusion protein on its own. Previous studies reported that collagen-binding BMP2 demonstrated ectopic bone formation when applied with bone-derived matrix as a scaffold.[22,23] Bone-derived matrix contains many factors, including native BMPs, and the complex is not fully defined, suggesting potential difficulties in clinical use. Second, CBD-BMP4 was effective even in a single low dose. In the present study, we injected 100 ng of CBD-BMP4 (≈2 pM), as preliminary experiments showed that BMP4 at this dose failed to induce appreciable bone formation at 4 weeks after the injection (not shown). Others used 8 nM CBD-BMP2 for ectopic bone formation model and 0.5 nM for the bone defect model.[24] Although verification of whether higher amounts of CBD-BMP4 could induce stronger bone formation in a critical-sized bone defect remains to be completed, we believe that our results predict that CBD-BMP4 will be very efficient with larger doses. In a bone-defect model, 2.5 μg to 5 μg of recombinant BMP4 was applied with collagen sponge or beta-tricalcium phosphate.[11] We believe our initial results also predict that, compared to other reagents, the CBD-BMP4 fusion protein will efficaciously require reduced amounts of protein to induce bone formation and thus limit possible clinical complications.

It appears that CBD-BMP4 both directly and indirectly induced bone formation. We have demonstrated that CBD-BMP4 induced osteogenic differentiation using three-dimensional cultures of human bone marrow-derived mesenchymal stem cells.[15] As shown in this study, CBD-BMP4 treatment upregulated the expression of all relevant osteogenic genes examined in the target site, even after 4 weeks postinjection, possibly due to the continued functional localization of the fusion protein. ALP is a major biomarker of bone formation and plays a key role in bone mineralization.[25] BSP is upregulated as osteoblasts mature at sites of de novo bone formation.[26] Osteocalcin is an ECM protein and among the most specific markers for osteoblast maturation.[27] Osterix is a bone-related transcription factor that functions genetically downstream of Runx2, which regulates the differentiation and/or function of osteoblasts.[28,29] In addition, CBD-BMP4 increased the expression of endogenous BMP2 and BMP4. Thus, CBD-BMP4 stimulated de novo expressions of osteogenic genes and bone growth factors for a longer period and initiated the calcification of the ECM, leading to the prolonged bone formation.

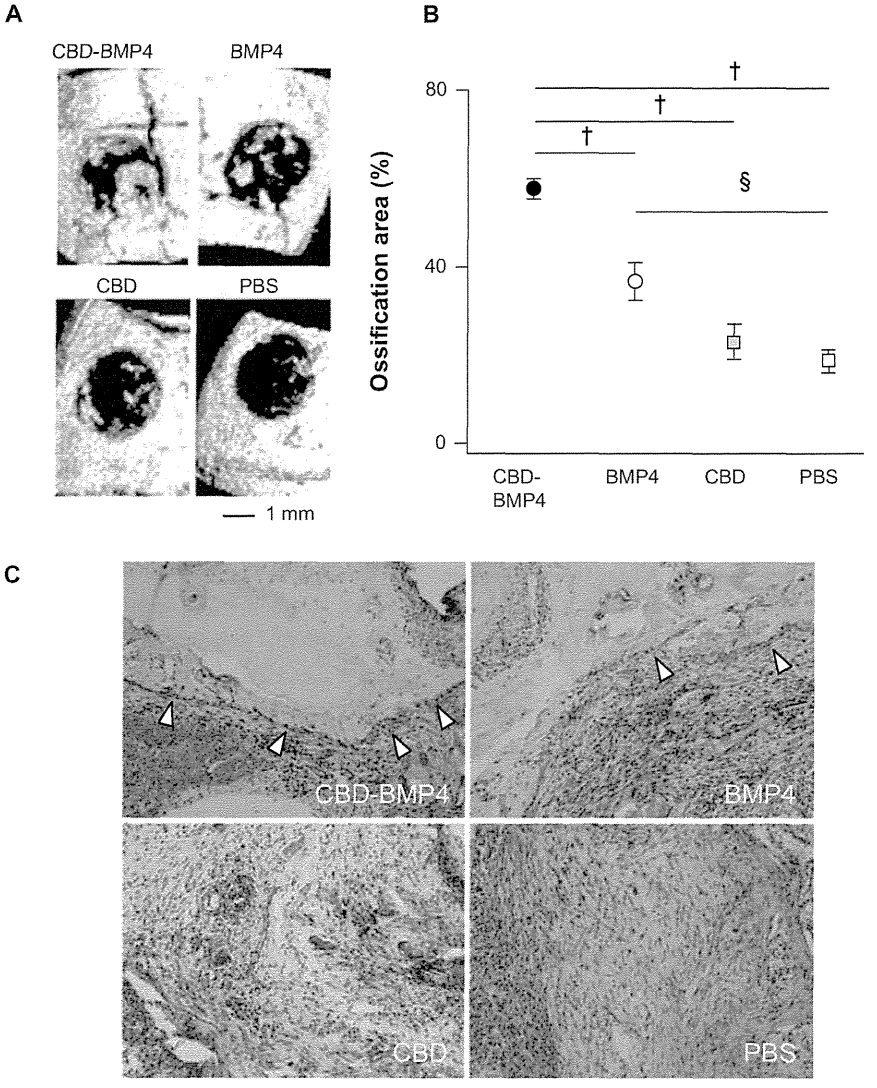

Figure 7 CBD-BMP4 enhances bone formation in a cranial bone defect model. CBD-BMP4, BMP4, CBD (100 ng in 5 μL PBS), or vehicle PBS (5 μL) was applied to the defective section of cranial bone (five mice per each group). At 2 weeks after the injection, the mice were killed, and the bone defects were scanned by micro-CT. (**A**) Representative three-dimensional CT images from each group. (**B**) Ossification area was calculated by micro-CT. $^{\S}P < 0.05$; $^{\dagger}P < 0.01$. (**C**) Representative tissue sections from each group are shown (HE staining).

Note: Arrowheads indicated the layer of osteoblasts.

Abbreviations: CBD, collagen-binding domain; BMP4, bone morphogenetic protein-4; PBS, phosphate buffered saline; CT, computed tomography; HE, hematoxylin and eosin stain.

Of note was the finding that CBD by itself somewhat induced bone formation when intramedullary injected. Similar to CBD-BMP4, CBD remained at the injected site. The CBD used in this fusion protein was from fibronectin,[17] which is an ECM component. ECMs and growth factors function cooperatively to stimulate osteoblast differentiation. There is evidence to suggest a role for fibronectin in the early stages of bone formation.[30,31] Recently, it has been demonstrated that ECMs including fibronectin modified the growth patterns and induced the osteoblast differentiation of human myeloid stem cells, as evidenced by increased expressions of ALP, osteocalcin, osterix, and Runx2.[32] Accordingly, we showed in this study that CBD upregulated the expressions of osteogenic genes such as ALP, BSP, and osteocalcin, and growth factor BMP4. Although CBD is a segment (amino acids 260–599) of the original fibronectin,[15] CBD may contain fibronectin's active site leading to osteogenesis. Thus, the osteogenic capacity of CBD-BMP4 may be partly due to the activity of CBD. A question arises as to whether the simultaneous injection of CBD and BMP4 could represent additive

or synergistic osteogenic effects, which was not examined in this study. CBD-BMP4 had no osteogenic effects when applied to the defective section of cranial bone. The disparity may be due to the different location of the given site (bone marrow versus cortical bone).

There are several other concerns that were not confronted in this study. Although we believe that CBD-BMP4 binds to bone matrix collagen at the injection site, we have not shown direct evidence. It is not clear how CBD-BMP4 interacts with the BMP4 receptor at the site and how CBD-BMP4 itself affects the surrounding cells, either when acting as a complex or as individual components. CBD-BMP4 has a higher molecular weight than BMP4, which may contribute to the physics of diffusion. Further studies are necessary to explore these precise mechanisms.

Conclusion

In conclusion, our engineered CBD-BMP4 is a novel fusion protein with an exquisite ability to promote in vivo osteogenesis, even by a single injection at the targeted site both with and without scaffold. There are many ways to enhance the release of BMP4 using chemical conjugation, particle vehicle, or gene delivery, which are low cost, verified, and convenient. We believe that our fusion protein is better than others, as CBD-BMP4 can localize longer at the designated site, resulting in stronger bone formation by a single low dose of complex. This novel CBD-BMP4 may be promising clinically for the treatment of unresolved fractures, bone defects, and other bone tissue engineering and regeneration-related scenarios.

Acknowledgments

We thank Takayuki Furumatsu, Reina Tanaka, and Yuki Nakashima for their excellent technical assistance. We also thank Judith Connett (University of Michigan Medical School, Ann Arbor, MI, USA) for her critical reading of the manuscript. This work was supported in part by grants from Ministry of Education, Culture, Sports, Science and Technology, Japan, and the Japan Society for the Promotion of Science, Grant-in-Aid for Scientific Research (S) of KAKENHI 22220009.

Disclosure

The authors report no conflicts of interest in this work.

References

1. Cierny G 3rd, Zorn KE. Segmental tibial defects. Comparing conventional and Ilizarov methodologies. *Clin Orthop Relat Res*. 1994; 301:118–123.
2. Myeroff C, Archdeacon M. Autogenous bone graft: donor sites and techniques. *J Bone Joint Surg Am*. 2011;93(23):2227–2236.
3. Linkhart TA, Mohan S, Baylink DJ. Growth factors for bone growth and repair: IGF, TGF beta, and BMP. *Bone*. 1996;19(Suppl 1):1S–2S.
4. Chen D, Zhao M, Mundy GR. Bone morphogenetic proteins. *Growth Factors*. 2004;22(4):233–241.
5. Marsell R, Einhorn TA. The role of endogenous bone morphogenetic proteins in normal skeletal repair. *Injury*. 2009;40 Suppl 3:S4–S7.
6. McKay WF, Peckham SM, Badura JM. A comprehensive clinical review of recombinant human bone morphogenetic protein-2 (INFUSE Bone Graft). *Int Orthop*. 2007;31(6):729–734.
7. White AP, Vaccaro AR, Hall JA, Whang PG, Friel BC, McKee MD. Clinical applications of BMP-7/OP-1 in fractures, nonunions, and spinal fusion. *Int Orthop*. 2007;31(6):735–741.
8. Anderson CL, Whitaker MC. Heterotopic ossification associated with recombinant human bone morphogenetic protein-2 (infuse) in posterolateral lumbar spine fusion: a case report. *Spine (Phila Pa 1976)*. 2012;37(8):E502–E506.
9. Joseph V, Rampersaud YR. Heterotopic bone formation with the use of rhBMP2 in posterior minimal access interbody fusion: a CT analysis. *Spine (Phila Pa 1976)*. 2007;32(25):2885–2890.
10. Kim PD, Ludwig S, Poelstra K, Duggan B, Scalea T, Gelb D. Ectopic bone formation in the pelvis after combined anterior and posterior fusion of the spine with osteogenic protein-1 use: a case report. *J Spinal Disord Tech*. 2010;23(3):215–220.
11. Pang EK, Im SU, Kim CS, et al. Effect of recombinant human bone morphogenetic protein-4 dose on bone formation in a rat calvarial defect model. *J Periodontol*. 2004;75(10):1364–1370.
12. Leong LM, Brickell PM. Bone morphogenic protein-4. *Int J Biochem Cell Biol*. 1996;28(12):1293–1296.
13. Rundle CH, Miyakoshi N, Kasukawa Y, et al. In vivo bone formation in fracture repair induced by direct retroviral-based gene therapy with bone morphogenetic protein-4. *Bone*. 2003;32(6):591–601.
14. López-Morales Y, Abarrategi A, Ramos V, et al. In vivo comparison of the effects of rhBMP-2 and rhBMP-4 in osteochondral tissue regeneration. *Eur Cell Mater*. 2010;20:367–378.
15. Lu H, Kawazoe N, Kitajima T, et al. Spatial immobilization of bone morphogenetic protein-4 in a collagen-PLGA hybrid scaffold for enhanced osteoinductivity. *Biomaterials*. 2012;33(26):6140–6146.
16. Price TM, Rudee ML, Pierschbacher M, Ruoslahti E. Structure of fibronectin and its fragments in electron microscopy. *Eur J Biochem*. 1982;129(2):359–363.
17. Ishikawa T, Terai H, Kitajima T. Production of a biologically active epidermal growth factor fusion protein with high collagen affinity. *J Biochem*. 2001;129(4):627–633.
18. Kawamoto T, Shimizu M. A method for preparing 2- to 50-micron-thick fresh-frozen sections of large samples and undecalcified hard tissues. *Histochem Cell Biol*. 2000;113(5):331–339.
19. Aalami OO, Nacamuli RP, Lenton KA, et al. Applications of a mouse model of calvarial healing: differences in regenerative abilities of juveniles and adults. *Plast Reconstr Surg*. 2004;114(3):713–720.
20. Robey PG, Fedarko NS, Hefferan TE, et al. Structure and molecular regulation of bone matrix proteins. *J Bone Miner Res*. 1993;8 Suppl 2: S483–S487.
21. Kitajima T, Ito Y. Artificial binding growth factors. In: Khang G, editor. *Handbook of Intelligent Scaffolds for Tissue Engineering and Regenerative Medicine*. Singapore: Pan Stanford Publishing; 2012: 337–353.
22. Chen B, Lin H, Zhao Y, et al. Activation of demineralized bone matrix by genetically engineered human bone morphogenetic protein-2 with a collagen binding domain derived from von Willebrand factor propolypeptide. *J Biomed Mater Res A*. 2007;80(2):428–434.
23. Zhao Y, Chen B, Lin H, et al. The bone-derived collagen containing mineralized matrix for the loading of collagen-binding bone morphogenetic protein-2. *J Biomed Mater Res A*. 2009;88(3):725–734.
24. Chen B, Lin H, Wang J, et al. Homogeneous osteogenesis and bone regeneration by demineralized bone matrix loading with collagen-targeting bone morphogenetic protein-2. *Biomaterials*. 2007;28(6): 1027–1035.

25. Anderson HC, Sipe JB, Hessle L, et al. Impaired calcification around matrix vesicles of growth plate and bone in alkaline phosphatase-deficient mice. *Am J Pathol*. 2004;164(3):841–847.
26. Bianco P, Riminucci M, Bonucci E, Termine JD, Robey PG. Bone sialoprotein (BSP) secretion and osteoblast differentiation: relationship to bromodeoxyuridine incorporation, alkaline phosphatase, and matrix deposition. *J Histochem Cytochem*. 1993;41(2):183–191.
27. Galli M, Caniggia M. Osteocalcin. *Minerva Med*. 1984;75(42): 2489–2501. Italian.
28. Nakashima K, Zhou X, Kunkel G, et al. The novel zinc finger-containing transcription factor osterix is required for osteoblast differentiation and bone formation. *Cell*. 2002;108(1):17–29.
29. Nishio Y, Dong Y, Paris M, O'Keefe RJ, Schwarz EM, Drissi H. Runx2-mediated regulation of the zinc finger Osterix/Sp7 gene. *Gene*. 2006;372:62–70.
30. Moursi AM, Damsky CH, Lull J, et al. Fibronectin regulates calvarial osteoblast differentiation. *J Cell Sci*. 1996;109(Pt 6):1369–1380.
31. Moursi AM, Globus RK, Damsky CH. Interactions between integrin receptors and fibronectin are required for calvarial osteoblast differentiation in vitro. *J Cell Sci*. 1997;110(Pt 18):2187–2196.
32. Mathews S, Bhonde R, Gupta PK, Totey S. Extracellular matrix protein mediated regulation of the osteoblast differentiation of bone marrow derived human mesenchymal stem cells. *Differentiation*. 2012;84(2):185–192.

Hindawi Publishing Corporation
The Scientific World Journal
Volume 2013, Article ID 359109, 7 pages
http://dx.doi.org/10.1155/2013/359109

Hindawi

Research Article

Chondrocyte Differentiation of Human Endometrial Gland-Derived MSCs in Layered Cell Sheets

Waki Sekine,[1] Yuji Haraguchi,[1] Tatsuya Shimizu,[1] Masayuki Yamato,[1] Akihiro Umezawa,[2] and Teruo Okano[1]

[1] *Institute of Advanced Biomedical Engineering and Science, TWIns, Tokyo Women's Medical University, 8-1 Kawada-cho, Shinjuku-ku, Tokyo 162-8666, Japan*
[2] *Department of Reproductive Biology, National Center for Child Health and Development, 2-10-1 Okura, Setagaya-ku, Tokyo 157-8535, Japan*

Correspondence should be addressed to Teruo Okano; tokano@abmes.twmu.ac.jp

Received 4 September 2013; Accepted 7 October 2013

Academic Editors: P. Akhyari and R. Y. Kannan

Recently, regenerative medicine using engineered three-dimensional (3D) tissues has been focused. In the fields of cell therapy and regenerative medicine, mesenchymal stem cells (MSCs) are attractive autologous cell sources. While, in bioengineered tissues, a 3D environment may affect the differentiation of the stem cells, little is known regarding the effect of 3D environment on cellular differentiation. In this study, MSC differentiation in *in vitro* 3D tissue models was assessed by human endometrial gland-derived MSCs (hEMSCs) and cell sheet technology. hEMSC sheets were layered into cell-dense 3D tissues and were cultured on porous membranes. The tissue sections revealed that chondrocyte-like cells were found within the multilayered cell sheets even at 24 h after layering. Immunostainings of chondrospecific markers were positive within those cell sheet constructs. In addition, sulfated glycosaminoglycan accumulation within the tissues increased in proportion to the numbers of layered cell sheets. The findings suggested that a high cell density and hypoxic environment in 3D tissues by layering cell sheets might accelerate a rapid differentiation of hEMSCs into chondrocytes without the help of chondro-differentiation reagents. These tissue models using cell sheets would give new insights to stem cell differentiation in 3D environment and contribute to the future application of stem cells to cartilage regenerative therapy.

1. Introduction

Cell-based regenerative therapy has a potential for treating diseased/defective tissues and organs that are unable to be cured by conventional medical treatments including medicines and surgeries. Regenerative medicine using artificial tissue fabricated by scaffold-based tissue engineering has appeared as the second-generation therapy, and the clinical trials have been performed [1–4]. Scaffold-based tissue engineering has been currently based on a concept that three-dimensional (3D) biomaterials including polycaprolactone, collagen, gelatin, and so forth are used as an alternative to extracellular matrix (ECM) and cells are seeded into the materials.

Our laboratory has developed a scaffolds-free tissue engineering, "cell sheet engineering," using temperature-responsive culture surfaces, which can control the attachment and detachment of living cells by simple temperature changes [5–7]. Three-dimensional cell-sheet constructs fabricated by the technology are clearly cell-dense, and their functional junctions are tightly formed among cells within the tissues [8–10]. For example, cardiomyocytes in engineered 3D myocardial tissues coupled electrically and functionally via gap junctions, and the tissues can beat synchronously like the real heart [8, 10]. In addition, the authors have recently found that thicker tissue (the thickness of sextuple-layered cell sheets: more than 100 μm) was able to be fabricated by a 3D-tissue culture method on porous membrane,

where the thickness limitation of viable tissue depends on oxygen and nutrient gradients could be avoided [9]. The circumstances of the thicker cell-dense 3D tissue culture are thought to be quite different from those of monolayer two-dimensional (2D) culture.

Mesenchymal stem cells (MSCs), which are a type of somatic stem cells, are an attractive autologous cell source for cell-based regenerative therapy, since they have a strong ability to proliferate actively *in vitro* and differentiate into various cells including chondrocytes, osteocytes, adipocytes, skeletal myoblasts, cardiomyocytes, and so forth, with the treatments of optimal bioactive factors including cytokines or their surrounded circumstances [11–17]. In addition, those cells can be isolated easily from various tissues including bone marrow, adipose tissue, umbilical cord, amniotic fluid, peripheral blood, and so forth. Recently, some stem cells, which express surface antigens similar to those of bone marrow-derived MSCs, are isolated from human menstrual blood and endometrial gland [18].

Cells within a 3D culture system are reported to be significantly different from those in a 2D culture system in terms of their morphology, cell-cell interactions, surrounding ECM, proliferation rates, differentiation, and so forth. [19–21]. These differences may be affected by their different circumstances of oxygen, nutrients, growth factors, cell-cell and cell-matrix interactions, and so forth. Although, in 2D culture, oxygen tension, and the concentrations of nutrients and growth factors are unusually high, in 3D culture, cells are subject to multiple stimuli, namely, cytokines, growth factors, and proteins secreted from surrounding cells [22]. Cells are also affected by biochemical and mechanical interactions with ECM as well as direct cell-cell contacts [22].

In this study, cell-dense thicker 3D tissues were fabricated from human endometrial gland-derived MSC (hEMSC) sheets, and the differentiation of the stem cells within the tissue was assessed and analyzed.

2. Materials and Methods

2.1. Preparation and Layering of hEMSC Sheets. hEMSCs, which showed an adherent spindle-shape morphology, were cultured in Dulbecco's modified Eagle's medium (DMEM) (Sigma-Aldrich, St. Louis, MO, USA) supplemented with 10% fetal bovine serum (FBS) (Japan Bio Serum, Nagoya), 1% penicillin/streptomycin (Invitrogen, Carlsbad, CA, USA) [9, 18, 23]. hEMSC sheets were fabricated as previous reports [9, 10, 23]. Briefly, hEMSCs (1.0×10^6 cells) were cultured on a 35 mm diameter temperature-responsive culture dish (Upcell, CellSeed, Tokyo, Japan) for 4 days at 37°C, and the culture dish was placed in a CO_2 incubator at 20°C. A hEMSC sheet detached itself spontaneously within 30 min. The cell sheets were layered on a cell-culture insert (Becton, Dickinson and Company, Franklin Lakes, NJ, USA) having a track-etched PET membrane (the membrane pore size: 1 μm), because a previous report has shown that the cultivation of layered cell sheets on the porous membranes induces the improvement of cell viability and the fabrication of thicker tissues than that on normal culture surfaces [9]. The insert was set in a 6-well cell-culture insert companion plate (Becton, Dickinson and Company). Harvested cell sheets from temperature-responsive culture surfaces were layered on the membrane as described in previous reports [9]. Briefly, a cell sheet with media was gently aspirated into the tip of a pipette and was transferred onto the membrane, which was pretreated with FBS for more than 30 min. After the first cell sheet was spread, the media were aspirated, and the plate was incubated at 37°C for allowing the cell sheet to fully adhere to the membrane. To layer hEMSC sheets, the second sheet recovered from another temperature-responsive culture dish was layered onto the first cell sheet. By the same fashion, recovered cell sheets were successfully layered up to sextuple layer. The multilayered cell sheets were cultured for 24 h in a humidified atmosphere of 5% CO_2 at 37°C with 2 mL medium (DMEM supplemented with 10% FBS, 1% penicillin/streptomycin) in both insert and well.

2.2. Histological Analysis. After being incubated for 24 h, multilayered cell sheets on the porous membranes were fixed with 4% paraformaldehyde solution (Muto Pure Chemicals, Tokyo, Japan) at least for 1 day. Specimens were embedded in paraffin, sectioned, and stained with hematoxylin and eosin. Prepared specimens were observed by an optical microscope (ECLIPSE TE2000-U) (Nikon, Tokyo, Japan).

2.3. Immunohistochemistry. For detecting chondrocyte differentiation, the deparaffinized sections were also stained with the antibodies of chondrospecific markers: (1) monoclonal anti-human type II collagen (Cosmo Bio, Tokyo, Japan), which were diluted at 1 : 100 and (2) hyaluronan-binding protein (Seikagaku Corporation, Tokyo, Japan), which were diluted at 1 : 200. The detections of the immunoreactions were enhanced by a CSA II Biotin-free Tyramide Signal Amplication System (Dako Cytomation, Glostrup, Denmark) according to the manufacturer-suggested protocol. Hematoxylin was used for nuclear counterstaining. Prepared specimens were observed by the optical microscope.

2.4. Measurement of Sulfated Glycosaminoglycan Accumulation within Layered hEMSC Sheets. The accumulation of sulfated glycosaminoglycan (sGAG), which is the constituent of ECM in cartilage tissues, within layered hEMSC sheets was quantitated by a commercially available kit (Seikagaku Biobusiness, Tokyo, Japan), which is a colorimetric determination method using 1,9-dimethylmethylene blue.

2.5. Data Analysis. Data were expressed as the mean ± SD. Dunnett's test was performed to compare two groups.

3. Results and Discussion

3.1. Morphological Analysis of the Layered hEMSC Sheets. hEMSC sheets were layered into 3D tissues onto a porous membrane, and the differentiation kinetics of the stem cells within the cell sheet constructs were histologically examined. At 24 h after the cultivation of layered hEMSC sheets, the constructs were observed cross-sectionally. Because, after detaching from temperature-responsive culture dishes, a cell

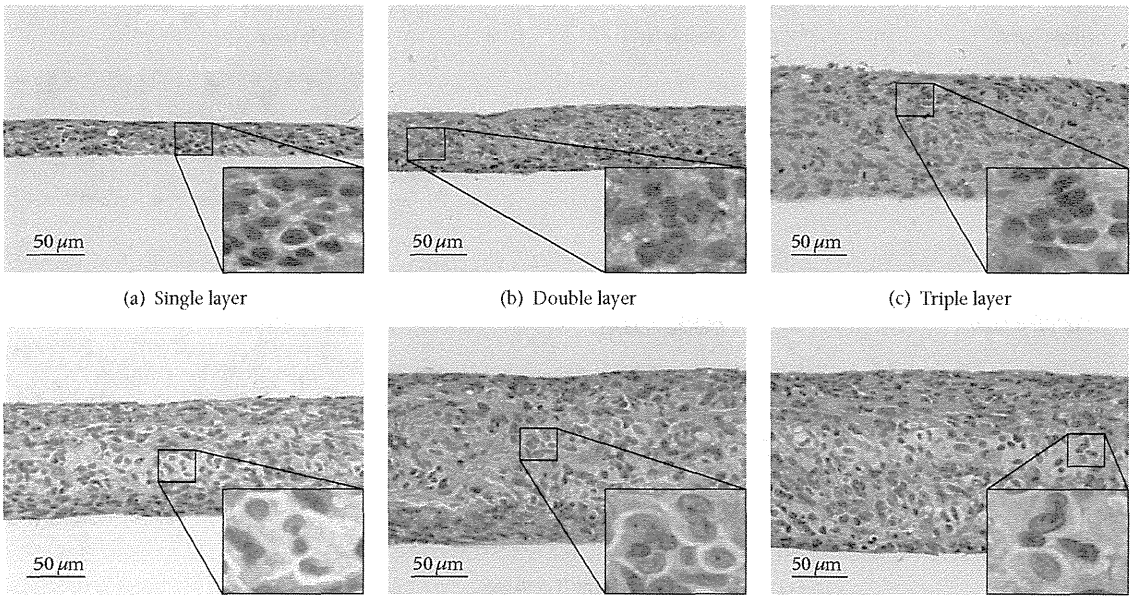

(a) Single layer (b) Double layer (c) Triple layer

(d) Quadruple layer (e) Quintuple layer (f) Sextuple layer

FIGURE 1: Histological observation of layered human endometrial gland-derived mesenchymal stem cells (hEMSC) sheets after a 24 h cultivation on porous membranes. All microphotographs are the hematoxylin and eosin stained cross-sections of the cell sheets ((a) single-layered cell sheet; (b) double-layered cell sheet; (c) triple-layered cell sheet; (d) quadruple-layered cell sheet; (e) quintuple-layered cell sheet; (f) sextuple-layered cell sheet). Enlarged photographs showed chondrocyte-like cells. Independent three experiments were performed and those experiments showed similar results. The representative photographs were shown in the figure.

sheet shrunk horizontally due to the cytoskeletal tensile reorganization, a single-layer cell sheet consisted of several cell-layers, and the thickness of the cell sheet became more than 25 μm (Figure 1). With increasing the number of stratified cell sheets, the thicknesses of the layered cell sheets increased as shown in Figure 1. The thicknesses of more than triple-layered cell sheets were more than 100 μm, and those cell layer tissues were clearly cell dense. Some characteristic cells were found within the multilayered cell-sheet constructs and resembled differentiated chondrocytes (Figure 1). Many chondrocyte-like cells were found within more than quadruple-layered cell-sheet constructs (Figures 1 and 2). After the cell sheet layering, hEMSCs might differentiate into chondrocytes very rapidly (24-h cultivation) within the multilayered cell sheet constructs. On the other hand, in single-, double-, triple-layered cell-sheet constructs, similar cell structures were observed (Figure 1).

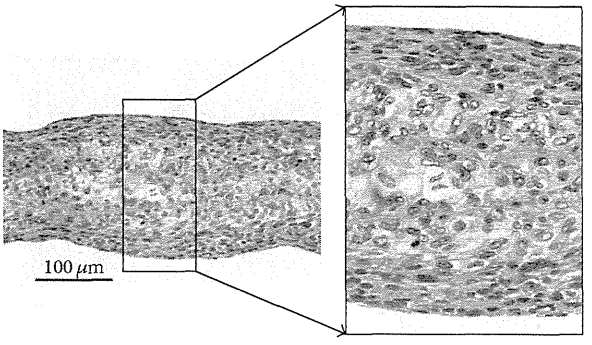

FIGURE 2: Histological observation of sextuple-layered hEMSC sheets. The left photograph is the cross-sectional observation of sextuple-layered cell sheets at 24 h after layering. The right is an enlarged photograph of the center part of the left photograph.

3.2. Expression of Chondrospecific Markers in Layered hEMSC Sheets. The expressions of chondrospecific markers in cells within 3D cell-sheet tissues fabricated by layering hEMSC sheets were examined by an immunohistological analysis. While, especially, the expression of type II collagen was strongly detected in multilayered (more than quadruple-layered) cell-sheet constructs, in all cell-sheet constructs including a single-layer cell sheet, the expression was detected (Figure 3(a)). Hyaluronan-binding protein was also expressed in all layered cell-sheets constructs (Figure 3(b)). These results confirmed the chondro-differentiation of hEMSCs within the multilayered cell sheet constructs. At the same time, the chondrocyte differentiation was suggested to occur in all cell-sheet constructs including a single-layer cell sheet. While those chondrospecific markers-positive cells were detected in the tissue constructs even at 24 h after the layering without the adding of chondro-differentiation reagents, no further increases were detected by further cultivation (data not shown). Those results were well consistent with that of morphological analysis (data not shown).

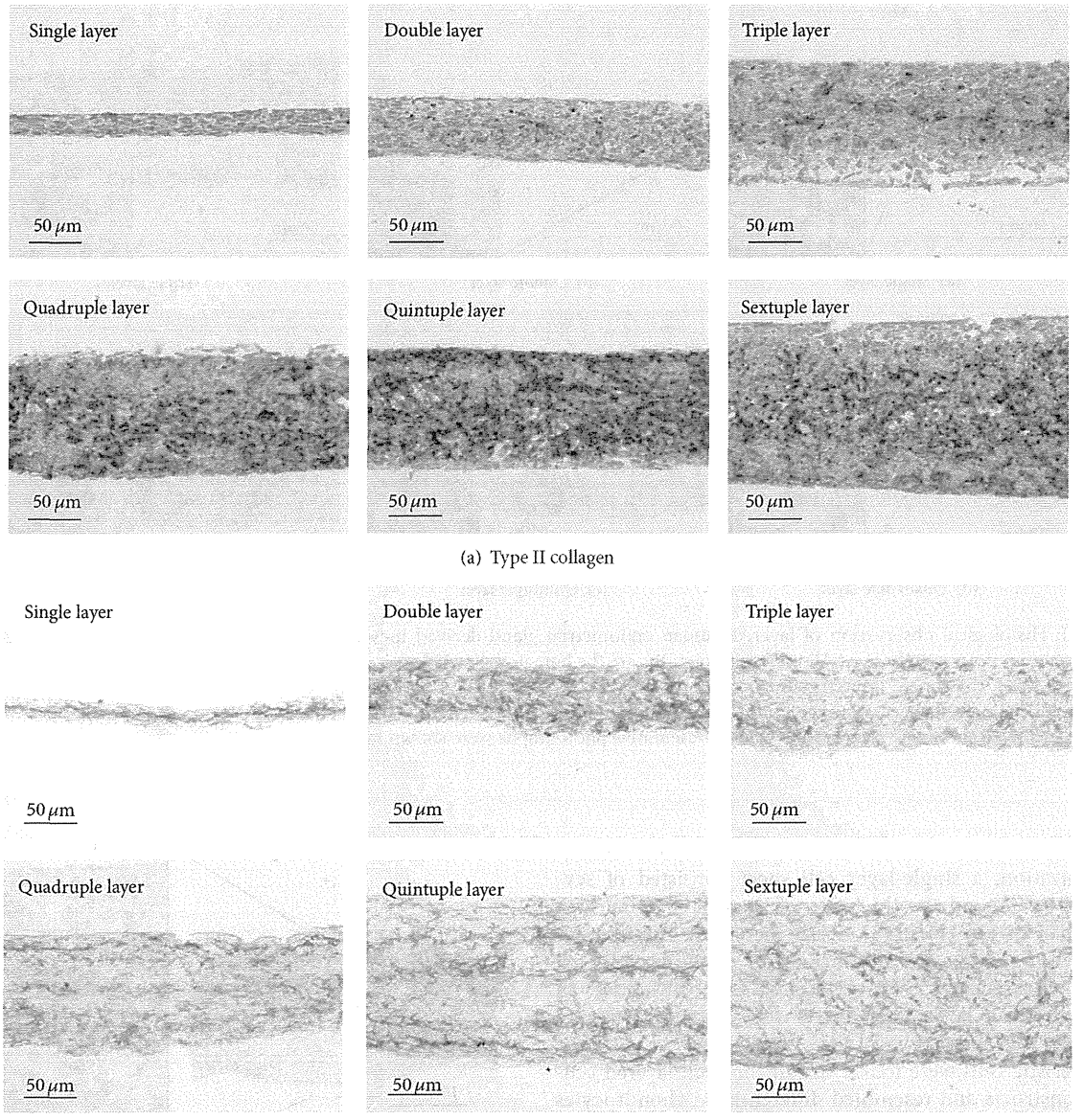

FIGURE 3: Detection of chondrospecific markers in layered cell sheet constructs at 24 h after layering by immunohistochemistry. Cells in single- and multilayered cell sheet constructs expressed type II collagen (a) and hyaluronan-binding protein (b).

sGAG accumulation within the constructs was measured quantitatively. The sGAG accumulations within cell sheets enhanced during a 24 h cultivation after detachment, and with increasing the number of stratified cell sheets (from single to sextuple), total sGAG accumulation tended to increase (Figure 4).

In this study, *in vitro* chondrocyte differentiation from hEMSCs within 3D tissue constructs fabricated by layering the stem cell sheets was shown. Articular cartilage has a poor ability for self-regeneration after the defective/injury, because it shows a low cell density and has limited blood supply. Various therapies including chondrocyte transplantation and tissue engineering methodology using 3D scaffolds have been performed clinically for regenerating articular cartilage damage [3, 24, 25]. For those therapies, autologous chondrocytes are isolated from the tissues and used as a cell source. At the same time, bone marrow-derived and adipose tissue-derived MSCs were also used as other autologous cell sources. MSCs differentiate into chondrocytes in the transplanted area *in vivo* and the implantation induces good therapeutic effects in animal models, and the therapies using bone marrow-derived MSCs have been clinically performed [17, 26–31]. This study suggested that hEMSCs as well as bone marrow-derived and adipose tissue-derived MSCs should be useful as

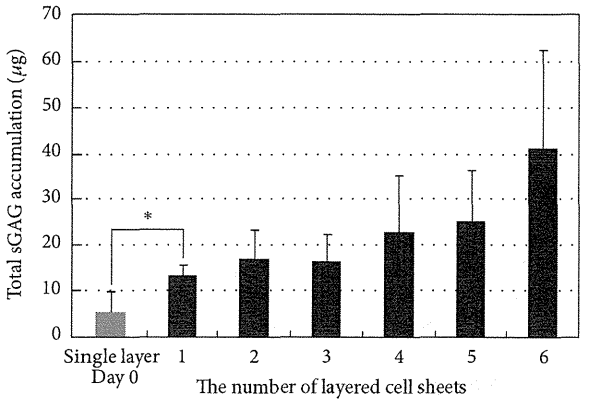

FIGURE 4: Detection of sulfated glycosaminoglycan (sGAG) accumulation within layered cell sheets at 24 h after the start of cultivation. With increasing the number of stratified cell sheets (from single to sextuple), sGAG accumulation increased. Data are shown as the mean ± SD ($n = 3$). The sGAG accumulations within a cell sheet enhanced during 24-h cultivation after detachment ($^*P < 0.05$).

a cell source for cartilage regenerative medicine. In addition, the chondrocyte differentiation of hEMSCs in 3D tissues fabricated by layering cell sheets was rapid (24 h cultivation after layering). Normally, *in vitro* differentiation from MSCs into chondrocytes is taken about for approximately three weeks by a conventional method [32]. Transplantation after the short term *in vitro* cultivation of layered hEMSC sheets into defective cartilage tissues might induce a stronger therapeutic effect than that of undifferentiated stem cells. On the other hand, although the expressions of chondrospecific markers were detected in the layered cell-sheet constructs even at 24 h, no further increases were detected by further cultivation (data not shown).

Cell sheet technology has now been applied to the regeneration of various damaged tissues, and clinical trials have been ready performed in several tissues including cornea epithelial, myocardial, esophageal, and periodontal tissues [33–37]. Because confluent cells on a temperature-responsive culture surface can be harvested as an intact and contiguous cell sheet by simply reducing the temperature without protease treatment, cell-cell junctions and ECM components mediating cell adhesion, which are susceptible to protease treatment, are preserved intact in the cell sheet [38–40]. Because cell sheets maintain cell-cell junctions and ECM components, cell-dense and functional 3D tissues can be easily fabricated by simply layering cell sheets without any scaffold, and the engineered tissues can also adhere directly to the host tissues without suturing [41]. More recently, the technology has been successfully applied to repair/regenerate the damaged cartilage tissue [42–46] and the clinical study has also been started. In *in vivo* and *ex vivo* experiments, multilayered human articular chondrocyte sheets were found to adhere firmly to rabbit and porcine cartilage tissues [42, 45]. The higher expressions of cell adhesion molecules, fibronectin and integrin $\alpha 10$ were detected in the multilayered chondrocyte sheets than those in monolayer chondrocytes [42, 44]. Layered chondrocyte sheets, which express highly those cell adhesion molecules, on temperature-responsive culture surfaces can be harvested by simply reducing culture temperature. In addition, scanning electron microscopical observation showed that the basal surface of the chondrocyte sheet had a completely different surface texture from that of the top of the sheet, and in other words, compared with the top surface, the bottom surface showed a smooth arrangement of the accumulated ECM with a parallel pattern [45]. The good adhesiveness of layered chondrocyte sheets onto the tissues might be related to the preservation of those molecules as well as the smooth arrangement of the basal surface, which more resembles normal cartilage surface than the top side of the cell sheet. Furthermore, while human articular chondrocytes is known to lose their chondrocyte phenotype during 2D cultivation [47], in the multilayered chondrocyte sheets, the expressions of chondrospecific markers, namely, type II collagen, SOX9, Aggrecan, are significantly increased in comparison to those in 2D cultured chondrocytes or in a single chondrocyte sheet, indicating that a multilayered chondrocyte sheet has a natural cartilage phenotype [42, 44]. The maintenance of chondrogenic phenotype might be related to the 3D environment of layered cell sheets. This study showed that an environment within 3D tissues fabricated by layering cell sheets might accelerate the differentiation of hEMSCs into chondrocytes. In the original and general chondrocyte differentiation methods from MSCs, the cells are collected into high cell-density pellets to induce a round shape and treated with cytokines/reagents described above [11–13]. In this study, the high cell density and hypoxic environment within 3D tissues might promote the chondrocyte differentiation of MSCs and the maintenance of chondrogenic phenotypes. *In vitro* cultivation under hypoxia has been reported to promote the restoration of chondrogenic phenotypes in human articular chondrocytes and enhance the chondrogenic differentiation of human bone marrow-derived MSCs [48, 49]. A previous report using a fiber-optical oxygen microsensor has showed that the oxygen concentrations between single- or multilayered EMSC sheets, and the insert membrane are quickly decreased, suggesting a hypoxia condition within layered cell sheets including single-layer cell sheets, whose thicknesses are more than 25 μm [9]. The elucidation of the detail molecular mechanisms of chondrocyte differentiation within 3D tissues should contribute to the establishment of novel and effective chondrocyte differentiation methods from MSCs and the fabrication of valuable 3D cartilage tissue. Layered cell sheets containing chondrocytes differentiated from hEMSCs on temperature-responsive culture surfaces were able to be harvested with preserving cell adhesive molecules on the cell surfaces and would contribute to cartilage tissue engineering and regenerative medicine.

4. Conclusion

This study assessed and analyzed human EMSC differentiation *in vitro* 3D tissue models using cell sheet technology. This study suggested that a high cell density and hypoxic environment in 3D tissues fabricated by layering cell